European Journal of Pharmaceutical Sciences 71 (2015) 46–55

Contents lists available at ScienceDirect

European Journal of Pharmaceutical Sciences

journal homepage: www.elsevier.com/locate/ejps

Silica nanoparticles: Preparation, characterization and *in vitro*/*in vivo* biodistribution studies

B.I. Tamba [a], A. Dondas [a], M. Leon [a], A.N. Neagu [b], G. Dodi [c,d], C. Stefanescu [e,*], A. Tijani [f]

[a] Centre for the Study and Therapy of Pain, "Gr. T. Popa" University of Medicine and Pharmacy, Iasi, Romania
[b] Laboratory of Animal Histology, Faculty of Biology, "Alexandru Ioan Cuza" University of Iasi, Romania
[c] Faculty of Chemical Engineering and Environmental Protection, "Gheorghe Asachi" Technical University of Iasi, Romania
[d] SCIENT – Research Centre for Instrumental Analysis, Bucharest, Romania
[e] Department of Biophysics and Medical Physics, "Gr. T. Popa" University of Medicine and Pharmacy, 700115 Iasi, Romania
[f] FHNW, School of Life Sciences, Switzerland

ARTICLE INFO

Article history:
Received 20 August 2014
Received in revised form 9 January 2015
Accepted 2 February 2015
Available online 11 February 2015

Keywords:
Silica nanoparticles
Fluorescent
Biodistribution
Microscopy
Scintigraphy

ABSTRACT

Background: The current progress in pharmaceutical nanotechnology field has been exploited in the design of functionalized radiolabelled nanoparticles that are able to deliver radionuclides in a selective manner to improve the outcome of diagnosis and treatment. Silica nanoparticles (SNPs) have been widely developed for biomedical applications due to their high versatility, excellent functional properties and low cost production, with the possibility to control different topological parameters relevant for multidisciplinary applications.
Purpose: The aim of the present study was to characterize and evaluate both *in vitro*, by microscopy techniques, and *in vivo*, by scintigraphic imaging, the biodistribution of silica nanostructures derivatives (Cy5.5 conjugated SNPs and ^{99m}Tc radiolabelled SNPs) to be applied as radiotracers in biomedicine.
Methods: SNPs were synthesized by hydrolysis and condensation of silicon alkoxides, followed by surface functionalization with amino groups available for fluorescent dye and radiolabelling possibility.
Results: Our data showed the particles size distribution (200–350 nm), the surface charge (negative for bare and fluorescent SNPs and positive for amino SNPs), polydispersity index (broad distribution), the qualitative composition and the toxicity assessments (safe material) that made the obtained SNPs candidates for *in vitro*/*in vivo* studies. A high uptake of fluorescent SNPs in all the investigated organs was evidenced by confocal microscopy. The ^{99m}Tc radiolabelled SNPs biodistribution was quantified in the range of 12–100% counts/g organ using the scintigraphic images.
Conclusions: The obtained results reveal improved properties, namely, reduced toxicity with a low level of side effects, an improved biodistribution, high labelling efficiency and stability of the radiolabelled SNPs with potential to be applied in biomedical science, particularly in nuclear medicine as a radiotracer.

1. Introduction

In the last period, the growing interest in molecular therapy is due to the possibilities offered by nanoparticles (NPs) as new tools for the delivery of therapeutic and target-specific drugs (Morales-Avila et al., 2012). Multifunctional radiolabelled nanoparticles provide an ideal platform to combine different approaches such as drug delivery with functional imaging techniques and used to target the site of the disease via both specific and non-specific mechanisms (Hong et al., 2009). Thus, novel strategies were explored for the radiolabelling of NPs in order to investigate the *in vivo* biodistribution in dependence with their architecture, size and structure (Md et al., 2013). In order to investigate the *in vivo* characteristics of NPs it has to be considered how they are interacting with tissues and cells, and especially which time frame allows a suitable visualization of certain effects and functions (Loudos et al., 2011). The necessity of creating radiolabelled nanocarriers is noticeable in all biomedical fields worldwide. Their fundament is anticipated to lead to advancements in understanding biological processes at the molecular level in addition to progress in the development of diagnostic tools and innovative therapies (Peer et al., 2007). Traditional radioisotope agents have certain disadvantages (instability, lack of specificity, low biodistribution, etc.) that must be improved by using new multifunctional radiolabelled structures (Garg et al., 2008; Newman et al., 2003).

* Corresponding author. Tel.: +40 232301615.
E-mail address: cipriana.stefanescu@yahoo.com (C. Stefanescu).

http://dx.doi.org/10.1016/j.ejps.2015.02.002
0928-0987/

Nanoparticles provide a large surface area and different types of functional groups available for bioactive agents or ligands attachment. Diverse nanomaterials with unique properties can be found in various biomedical applications, including *in vitro* or *in vivo* imaging, separation and purification of cells or biomolecules, and delivery of therapeutic agents. In the last two decades silica-based nanoparticles (SNPs) have gained increasing interest for medical applications because of their biocompatibility, versatility, stability, monodispersity, large surface area, high drug loading efficiency, and potential for hybridization with other materials (Argyo et al., 2014).

The surface of SNPs is usually negatively charged due to the presence of the hydroxyl group, therefore it is convenient to modify the SNPs' surface through the silane chemistry. In order to control the physico-chemical, toxicological and pharmacological properties, various reactive functional groups like amine, carboxyl, phosphate or polyethylene glycol could be easily conjugated to hydroxyl SNPs. Alternatively, the surface chemistry of the SNPs can be fine-tuned for a specific biological application, optimizing the dispersion stability and/or cellular uptake, the covalent attachment of imaging agents and targeting ligands the rational control of drug release rate (Mamaeva et al., 2013).

Numerous studies pointed toward their excellent potential as biomarkers, calibration standards in confocal fluorescence microscopy, drug delivery and targeting systems (tumor imaging and therapy *in vitro* and *in vivo*) in biomedical science (Legrand et al., 2008; Lu et al., 2007; Slowing et al., 2007). The imaging agents such as, fluorescein isothiocyanate, methylene blue, quantum dots, gadolinium chelates, tetramethylrhodamine or the targeting ligands, such as aptamers, antibodies, peptides, and folic acid, can be easily doped into or modified on the surface (Wu et al., 2014). Despite the growing body of papers related to the use of SNPs as therapeutic and imaging tool, today's challenge remains the biodistribution of silica nanostructures for *in vivo* diagnostic and therapeutic applications. This study focuses on the biodistribution of SNPs (fluorescent with Cy5.5 dye and radiolabelled with ^{99m}Tc, respectively) in rodents, in order to determine possible uses in therapeutic and/or diagnostic schemes. Due to the increasing health concerns regarding the use of nanoparticles in medical applications, and more specifically on amorphous silica nanoparticles, we also performed an acute toxicology screening of SNPs used in this study in order to evaluate their safety.

2. Materials and methods

2.1. Synthesis of SNPs

For this part of our study TEOS (tetraethyl orthosilicate), APTES (3-aminopropyltriethoxysilane), aqueous ammonia solution (NH_3, 28–30%), Cy5.5 reactive dye and ethanol (>99.9%) from Sigma Aldrich were used. All solutions were prepared with ultrapure water.

Four types of silica nanoparticles derivatives were synthesized and used for *in vitro*/*in vivo* evaluation, as follows:

- *Batch AA1:* bare SNPs were produced by hydrolysis and condensation of TEOS in ethanol in the presence of ammonia as a catalyst using a modified version of the method described by Stober et al. (1968). Briefly, a solution consisting of ammonia (25%) and water in 100 mL of ethanol was prepared. 0.28 M TEOS solution (in ethanol) was added at room temperature under vigorous stirring for 24 h. Finally, the colloidal solution was separated by centrifugation at 6000 rpm for 5 min and then washed with ethanol and ultrapure water for several times to remove the unreacted species.
- *Batch AA2:* the surface amine functionalization involved a standard procedure to synthesize the NH_2-SNPs. First, ethanol, ultrapure water and TEOS (0.28 M) mixtures were prepared, followed by addition of 0.14 M APTES in ethanol. The hydrolysis and co-condensation of TEOS and APTES was initiated by the addition of 1 mL of ammonia solution (25%) to the reaction mixture and stirred for 24 h at room temperature, resulting in the formation of the core–shell-NH_2-SNPs. Samples were then centrifuged (6000 rpm for 10 min) and washed with ethanol and ultrapure water.
- *Batch AA3:* the terminal amine groups from batch AA2 were used for the conjugation of Cy5.5, a near infrared (NIR) optical probe, using a mixture of Cy5.5 dye (commercially available with an N-hydroxysuccinimide ester group for binding to amine groups), ethanol and buffer solution (1 mg; 0.14 M) added under continuous stirring at room temperature for 6 h.
- *Batch ^{99m}Tc-SNPs:* amine surface-modified SNPs (batch AA2) were used for coupling ^{99m}Tc on the nanoparticle's surface as a radiotracer to study the biodistribution of the so-produced SNPs. Briefly, SNPs were suspended in ultrapure water (5 mg/mL) and dispersed by sonication for 15–20 min. An aqueous solution of $NaBH_4$ (reducing agent) was added under continuous stirring and homogenized for 1 h. Then, to the above mixture $^{99m}TcO_4^-Na$ solution was added quickly under vigorous stirring and left for another 30 min. The obtained product was separated by centrifugation and washed with ultrapure water to remove the uncoupled ^{99m}Tc radionuclide.

$^{99m}TcO_4^-Na$ (sodium pertechnetate) was chosen for labelling because it is the most commonly used emitting radioisotope in nuclear medicine having a convenient half-life of approximately 6 h, appropriate energy (140 keV) for imaging on a standard gamma camera and less attenuation by soft tissue. A 12.5 GBq Drytec Technetium Generator was used for the production of $^{99m}TcO_4^-Na$ supplied by GE Healthcare.

2.2. Characterization of the SNPs

SEM experiments were carried out at an accelerating voltage of 20 kV on a field emission scanning electron microscope (FE-SEM, Zeiss, SUPRA VP 40). Samples suspended in ultrapure water (1 mg/mL) were deposited on freshly cleaved mica surface, dried and gold/palladium coated.

Determinations of nanoparticles size, zeta potential and polydispersity index were performed using a Zetasizer (Zetasizer Nano ZS, Malvern Instruments). The samples were dispersed in ultrapure water and measured at a scattering angle of 90° and 25 °C. Qualitative chemical composition assessment of the nanoparticles was performed by FTIR analysis (Bomem MB 104 spectrometer). The material was finely grounded and dispersed into KBr powder-pressed pellets using a ratio of approximately 1 mg sample/200 mg KBr. IR absorbance data were obtained over a range of wavenumbers from 4000 to 400 cm^{-1}.

2.3. Experimental animals

All animals experimental procedures employed in the present study were strictly in accordance with the European Community Guidelines regarding ethics and approved by "Gr. T. Popa" University of Medicine and Pharmacy animal care and use committee. The animal breeding facility of the Central Drug Testing Laboratory, "Gr. T. Popa" University of Medicine and Pharmacy, Iasi, supplied adult male Swiss mice with an average weight of 20 ± 2 g and male guinea pigs with an average weight of 600 ± 50 g. The animals were housed in a temperature-controlled room (21 ± 2 °C) with a 12/12 h light/dark cycle, and given food and water ad libitum.

2.4. General toxicity screening

For acute systemic toxicity screening, three groups of mice (10 mice per dose) received intraperitoneal 0.1 mL SNPs buffer solution (batch AA3) in a single dose (25, 50 and 100 mg/kg body weight (bw)) and kept under observation for 5 days after administration. For all experiments, nanoparticles were ultrasonicated for 30 min directly prior to use. The maximum possible dose (20 mg SNPs per 1 mL PBS) administered was defined by preliminary experimental results – maximum tolerated dose (MTD) (Kong et al., 2011). The animals were carefully observed for obvious signs of toxicity, such as convulsions or body weight effects. All mice were necropsied to detect macroscopic evidence of organ and tissue damage or dysfunction.

2.5. Microscopy biodistribution studies

Fluorescent silica nanoparticles (batch AA3) (7.5 mg/1 mL PBS) were administered via two routes in 2 groups of 6 mice: intravenously (0.1 mL /mouse) and orally (0.2 mL/mouse). The control group (6 animals) received a similar volume of PBS. At specific times after intravenous (30 min and 2 h) or oral administration (1, 2, 24, 48 and 72 h) of the labelled nanoparticles (batch AA3) the mice were deeply anesthetized with xylazine and transcardially perfused with 15 mL 0.9% saline solution, followed by fresh 4% paraformaldehyde (PFA) in 75 mL 0.1 M PBS. Key organs (brain, heart, liver, lung, kidneys, spleen, testis and bladder) were extracted and post-fixed overnight in 4% PFA, followed by cryoprotection in 30% sucrose in PBS for 72 h. Sections of the above mentioned organs were cut using a freezing microtome (CM 1850 Leica Microsystems, Germany), were collected, mounted on slides and examined in a Leica Confocal Laser Scanning Microscope (TCS SPE DM 5500Q), using a laser diode (635 nm line), taking account that the Cy5.5 fluorochrome is optimally excited near 675 nm and fluoresces near 694 nm.

2.6. Scintigraphy biodistribution studies

^{99m}Tc radiolabelled NPs were used in order to study the biodistribution (batch ^{99m}Tc-SNPs).

Five groups of 4 male guinea pigs were injected with 37 MBq/kg bw of ^{99m}Tc-coupled amino SNPs. Jugular vein was exposed and cannulated for infusion of radiotracer.

A control group of 4 male guinea pigs received 37 MBq/kg bw of $^{99m}TcO_4^-Na$, in the same conditions. The guinea pigs were placed under a dual-head gamma camera (SPECT Siemens Gamma camera with LEAP (Low Energy All Purpose) collimators). The body distribution profile was recorded in dynamic mode till 5 min post injection and in static mode every 15 min for 2 h, then every 30 min for a total of 6 h.

The animals were sacrificed after 6 h and different organs were extracted and immediately gamma counted.

2.7. Statistical analysis

The experiments were replicated three independent times and the data are presented as ±SD (standard deviation). Statistical analysis was carried out using ANOVA followed by Bonferroni post hoc test. Differences were considered statistically significant when p-value was less than 0.05.

3. Results and discussion

3.1. SNPs design

Four types of SNPs were synthesized, as shown in Fig. 1 using a derived method with original modifications for the synthesis of spherical and monodisperse silica nanoparticles. First, SNPs

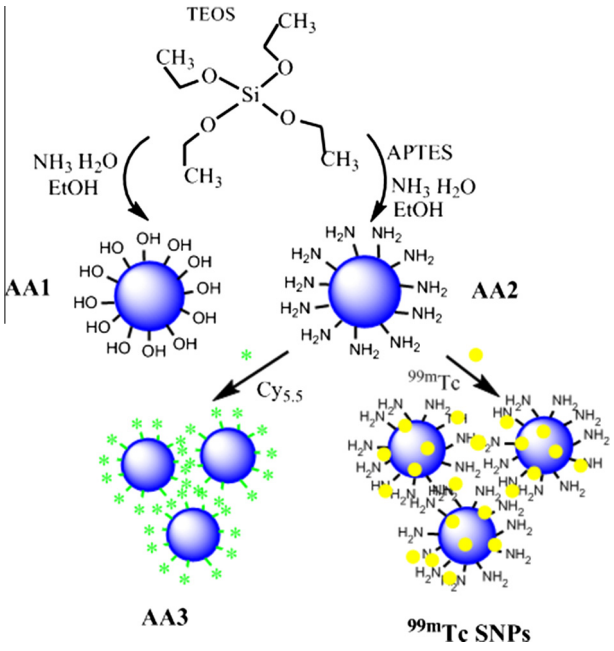

Fig. 1. Schematic presentation of SNPs design.

bearing OH groups were prepared from aqueous alcohol solutions of silicon alkoxides in the presence of ammonia as a catalyst by hydrolysis with the formation of silanol groups and condensation reaction for the siloxane bridges development (batch AA1). Since it is supposed that the binding affinity between the nanocarrier and the radioisotope along with the stability of the obtained radiotracer could be modulated by modifying the surface properties of the silica nanocarrier, functionalization via covalent bonding of organic groups was achieved by co-condensation of TEOS and APTES to obtain amine-functionalized silica nanoparticles with high specific surface area in a one-step reaction (batch AA2). The third type of SNPs involves a contrast agent attachment for biodistribution studies. Cy5.5 is a highly sensitive and bright cyanine dye with superior photostability compared to more commonly used dyes allowing more time for image detection. Cy5.5 is a good candidate for biological applications due to its stability and low non-specific binding. Cy5.5 is commercially available with an N-hydroxysuccinimide (NHS) ester group for binding to amine groups. Thus, SNPs comprising free amino group were used to conjugate Cy5.5 to the particle via active NHS ester.

In order to monitor their route *in vivo* and obtain an accurate biodistribution profile in each organ, NH_2-SNPs were labelled with a gamma emitting radioisotope, 99m-technetium (^{99m}Tc). Thus, the amino functionalized SNPs (batch AA2), selected for their enhanced surface reactivity, were first labelled with ^{99m}Tc radionuclide and then tested in healthy control groups for their visualization and tracking by gamma scintigraphy. The radionuclide ^{99m}Tc is commonly used as a radioisotope-tracer for diagnosis in nuclear medicine because it radiates gamma rays and is suitable for labelling different vector molecules.

Physicochemical characterization was performed only on bare, amino and fluorescent SNPs (batches AA1, AA2 and AA3), further studies will be performed regarding the mechanism of labelling between the amino groups and ^{99m}Tc, their size, surface charge and stability of the formed complex (Sarparanta et al., 2011).

3.2. Physico-chemical properties of SNPs

The surface structure and morphology of SNPs were investigated using FE-SEM. Fig. 2 shows SNPs as fairly uniform spherical

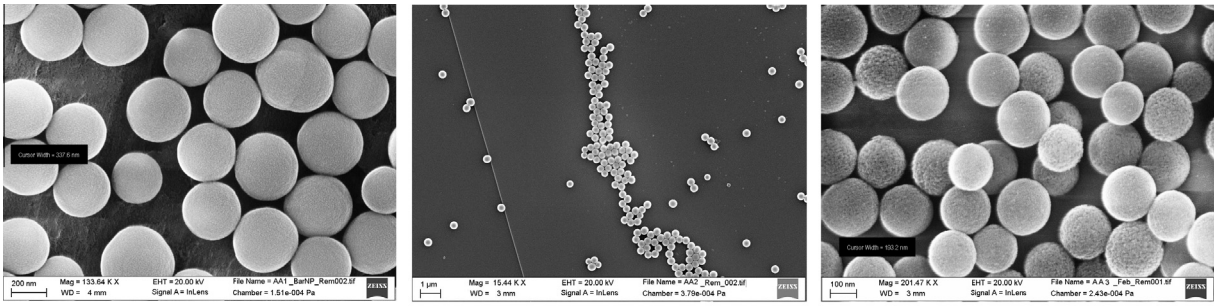

Fig. 2. FE-SEM images of A. bare SNPs (batch AA1); B. amino SNPs (batch AA2) and C. fluorescent SNPs (batch AA3).

Table 1
Size distribution, zeta potential and PDI data of SNPs derivatives.

Batch	Z-average hydrodynamic diameter (nm)	Zeta potential (mV)	PDI
AA1	408 ± 0.91	−37.8 ± 13.8	0.26
AA2	384 ± 0.72	+23.2 ± 3.6	0.12
AA3	460 ± 0.89	−25.5 ± 4.91	0.53

particles with an average size of 200–300 nm. FE-SEM image of spherical bare SNPs with a mean particle diameter of 300 ± 5 nm (batch AA1) is presented in Fig. 2A. Fig. 2B shows the amino-functionalized SNPs (batch AA2) with a narrow particle size distribution of about 250 ± 2 nm. After the Cy5.5 dye attachment on the amino groups, SNPs decreased in size to about 200 ± 2 nm due to the shrinking and partial dissolution of the particle, according to the FE-SEM pictures. The morphology and size distribution of Cy5.5 labelled SNPs (batch AA3) are shown in Fig. 2C.

In agreement with FE-SEM results, dynamic light scattering measurements evidenced (Table 1) the increase of the apparent hydrodynamic diameter when dispersed in aqueous solution. The large diameter (Table 1) might be explained by the polydispersity of the sample and indirectly confirms the presence of aggregates formed in the presence of water, which modifies the particles' lipophilic character by increasing the hydrophilic balance.

In order to evaluate the surface properties of the produced SNPs, zeta potential measurements were performed. As expected, bare SNPs showed negative zeta potential values (−38.7 mV) due to the silanol groups, which is in agreement with previous studies (Digigow et al., 2014). Upon addition of APTES, the zeta potential increases to a positive value of +23.2 mV, which is attributed to the appearance of the protonated amine ($-NH_3^+$) groups (p*K*a = 9) on the nanoparticle surface. The zeta potential measurements of samples made with Cy5.5 dye showed a negative value (−25.5 mV), which could come from negative charges of the carboxyl groups and the disappearance of the amino moieties.

The polydispersity index (PDI) describes the width of the assumed Gaussian distribution of the SNPs. The obtained dimensionless values indicate that the samples have a broad size distribution since PDI > 0.1, fact explained by the dispersion of the nanoparticles in water.

Additional stability studies were performed in order to evaluate the strength of the SNPs in biological environment over 240 min. The obtained results demonstrate that the bare, amino and fluorescent SNPs tend to form large aggregates when dispersed in water, therefore, the hydrodynamic diameter is increasing over

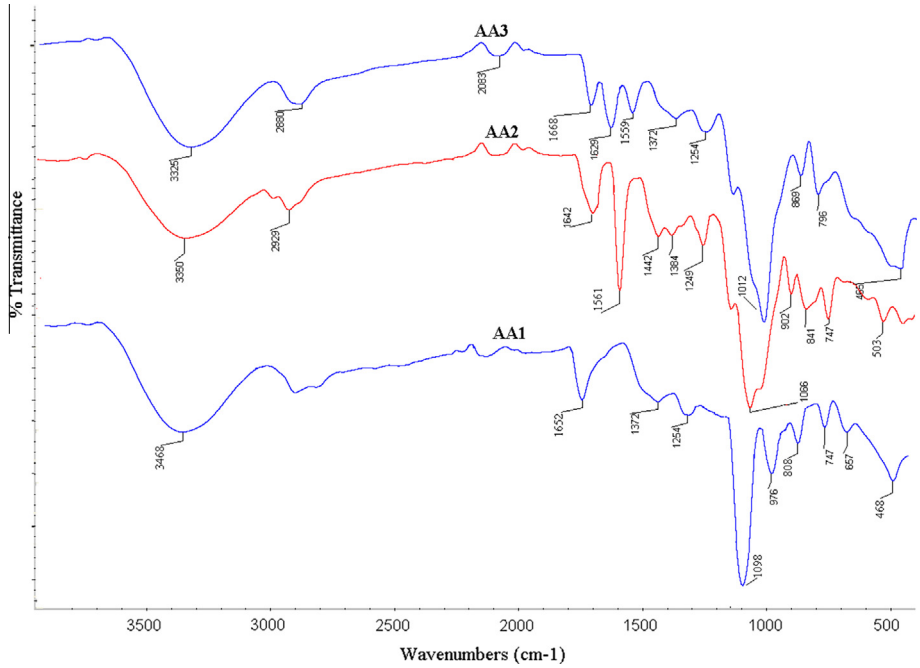

Fig. 3. FT-IR of bare SNPs (batch AA1), amino SNPs (batch AA2) and fluorescent SNPs (batch AA3).

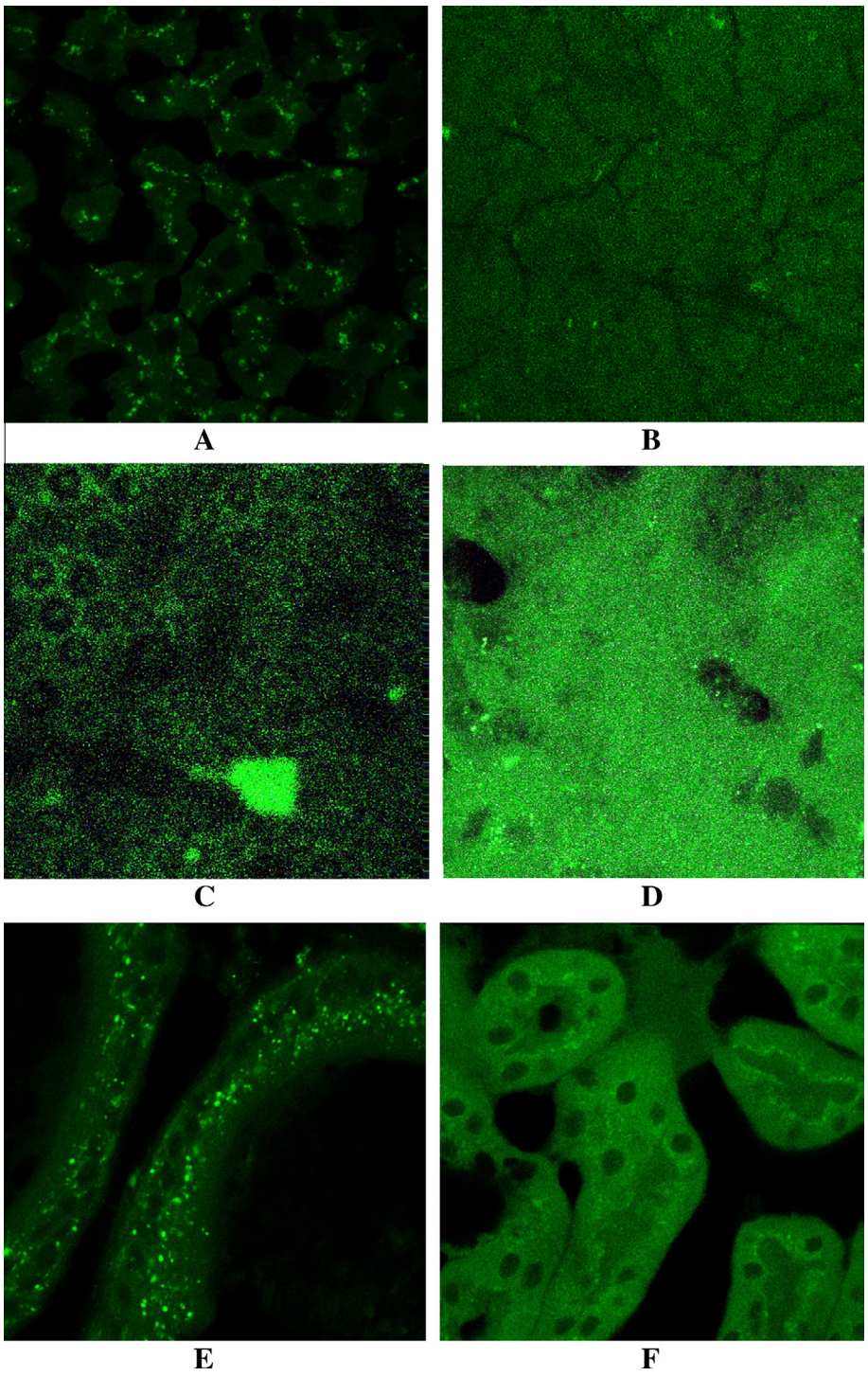

Fig. 4. SNPs distribution in A. Liver; B. Liver control; C. Lung; D. Feces; E. Testis and F. Kidney (2 h after intravenous administration – batch AA3; 630×).

time. Further studies must be conducted in order to optimize the *in vitro* serum stability of the radiolabelled complexes.

FT-IR measurements were performed to identify the structural differences between bare, amino and fluorescent SNPs. Fig. 3 illustrates the FT-IR spectra of all samples in the range of 400–4000 cm^{-1}. The bare SNPs (batch AA1) exhibited IR peaks at the bands attributed to Si-O-Si bending (468 cm^{-1}), Si-O-Si symmetric stretching (808 cm^{-1}), external Si-OH groups (976 cm^{-1}), Si-O-Si asymmetric stretching (1098 cm^{-1}), water molecules retained by siliceous materials (1652 cm^{-1}), and -OH stretching (3468 cm^{-1}) (Kamarudin et al., 2013). After modification with APTES, the SNPs still retained its siliceous structure, displaying no major changes in the formation of NH_2-SNPs (batch AA2). The new absorption band at 1561 cm^{-1} is attributable to a NH_2 scissor vibration, suggesting the presence of the amino groups of APTES molecules. Also, compared with the bare SNPs, the APTES-modified SNPs show an additional weak band at 2929 cm^{-1}, which can be assigned to the alkyl groups [$-(CH_2)_n-$] present in APTES.

After cyanine dye attachment, the relative intensity of amine group vibrations became less intense, suggesting that Cy5.5 was successfully loaded onto the surface of SNPs. New bands at 1668 cm^{-1}, and 1629 cm^{-1} appeared after the loading process,

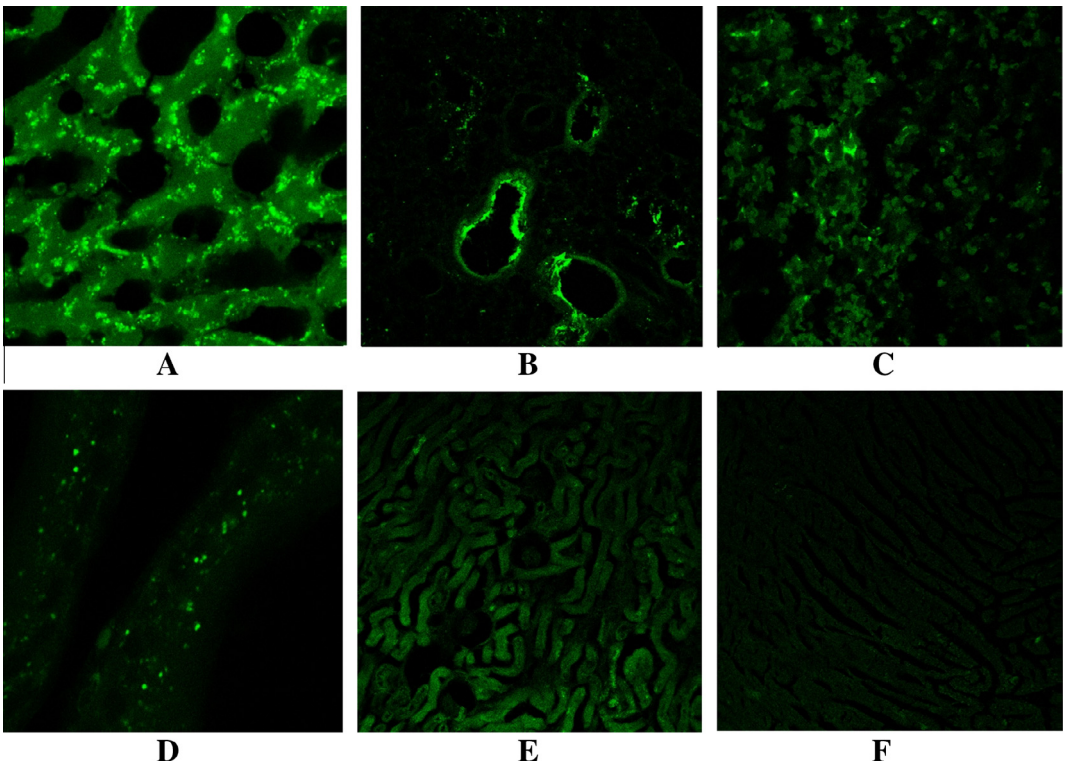

Fig. 5. SNPs distribution in A. Liver; B. Lung; C. Spleen; D. Testis; E. Kidney and F. heart (2 h after oral administration – batch AA3; 630×).

which might be associated with the aqueous solution of Cy5.5, and N-H group. All these facts suggest that Cy5.5 has been successfully attached to the surface of the NH_2-SNPs.

3.3. Toxicity evaluation

Nanoparticle toxicity has been shown to occur in a concentration-dependent manner (Lewinski et al., 2008). The determination of the appropriate dose of SNPs to use in a cytotoxicity assay is a key element to understand the toxic effects of the nanoparticles under true physiological conditions (Kong et al., 2011).

Although amorphous SNPs are commonly used as an FDA-approved food additive (Barnes et al., 2008) there are still numerous cytotoxicity studies raising concern about their toxic effects for human health: over exposure to amorphous SNPs has been shown to cause cytotoxic damage (as indicated by lactate dehydrogenase release) and a decrease in endothelial cell survival (Napierska et al., 2009).

According to the data obtained by Napierska et al. (2009), the toxicity of the SNP is size dependent, the smaller particles (diameters less than 15 nm), appear to affect the exposed cells faster with cell death, compared with larger ones (diameters of 104 and 335 nm) that showed low toxicity response. Also, the toxic effects depend on the nanoparticle's shape, charge and density, as well as the viscosity and density of the solution, properties that influence the effective dose. As a result, defining the appropriate dose for *in vitro*/*in vivo* study is still a challenging task.

In this study, fluorescent SNPs were used for general toxicity assessment. The acute toxicity screening allowed identifying the dose of 100 mg/kg bw as MTD for this study, with no significant changes in animal behavior or weight.

The histological examination (data not shown) of main organ tissue (liver, kidney, heart, stomach and intestine) that followed the five days observation period identified no histological changes from the normal tissues characteristics. The MTD was several times higher than the doses administered in the bioavailability studies, profiling a good safety profile for future therapeutic associations of the SNPs with drugs.

3.4. Biodistribution of the fluorescent SNPs by microscopy

The therapeutic efficiency of a drug carrier does rely not only on its intrinsic activity but also on the bioavailability of the drug at targeted site. In the development of novel therapeutics, the ability to design a suitable pharmaceutical formulation for delivery is of utmost importance.

Following the intravenous administration of fluorescent SNPs, batch AA3 (size 200 nm), at specific time points (30 min and 2 h) the SNPs did not penetrate the blood brain barrier and were not present in the myocardium. Bladder tissue sample were also negative. However, SNPs were found in the rest of the investigated organs (liver, kidney, testis, feces and lung, see Fig. 4).

In order to validate the obtained results, the organs of the control groups were also evaluated after PBS administration. Fig. 4B represents the comparative control liver examination at 2 h in the same conditions as the SNPs. The image evidenced the autofluorescence that was taken into consideration for the evaluation of the SNPs biodistribution as an example. The same pattern was observed also for the control images taken for both intravenously and oral administration of the fluorescent SNPs.

The biodistribution studies were performed also after the oral administration at specific time points (1 and 2 h). The SNPs were present in all the investigated organs (liver, kidney, testis, spleen, and lung) except the brain and heart (Fig. 5). However, we also found that significant amounts of SNPs were distributed at 24 and 48 h after administration, especially in the liver. After 72 h a gradually decrease of SNPs accumulation in liver and spleen was noticed.

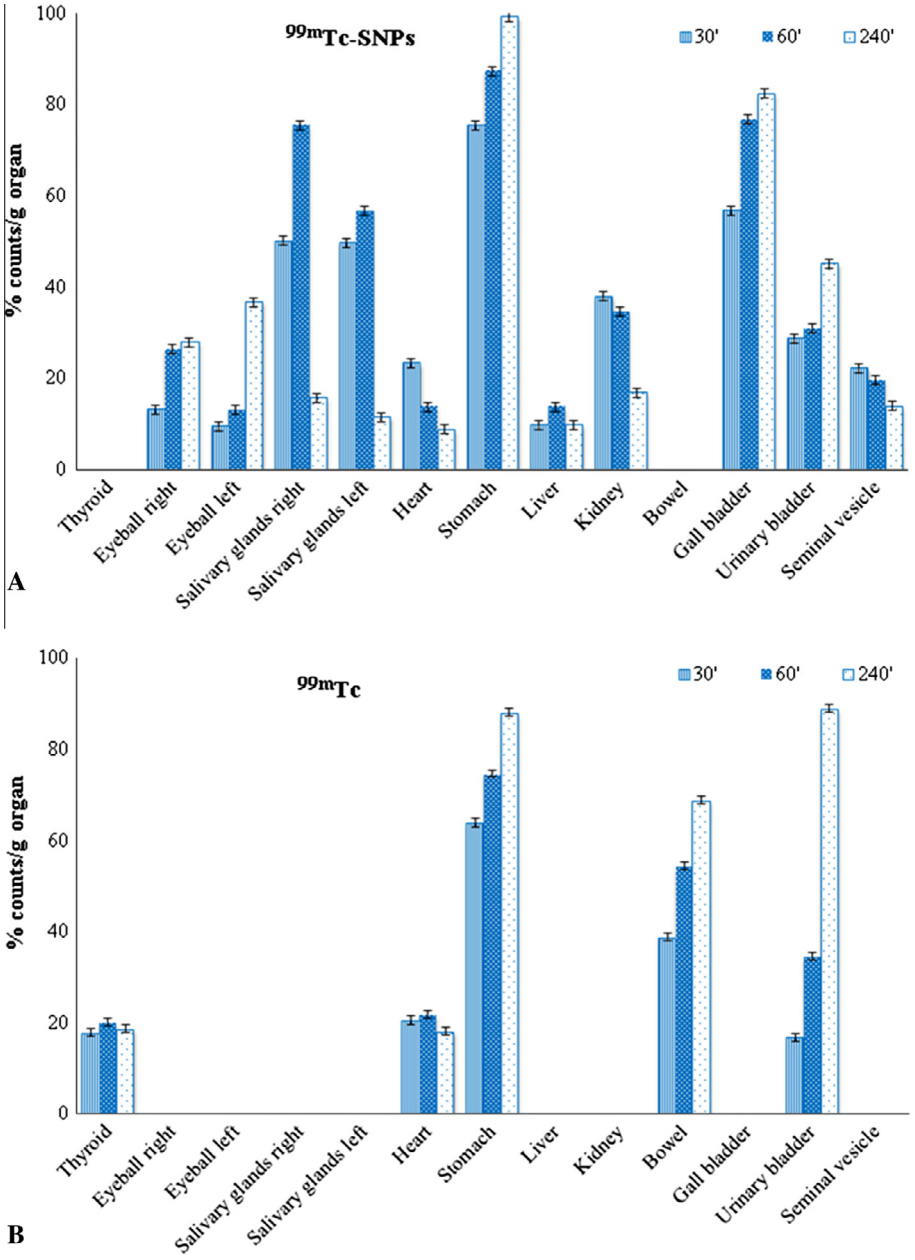

Fig. 6. Graphic biodistribution profile in different tissues at the times: 30, 60 and 240 min of A. ^{99m}Tc-SNPs and B. ^{99m}Tc. Values expressed as mean ± SD.

3.5. Biodistribution of the radiolabelled SNPs by scintigraphy

Although there are some studies in the literature about the qualitative *in vivo* distribution of SNPs, quantitative distribution data are still lacking. In our study, the fixation degree of the ^{99m}Tc-SNPs in different living structures (thyroid, eyeball right and left, salivary glands right and left, heart, stomach, liver, kidney, bowel, gall bladder, urinary bladder and seminal vesicle), at different time intervals was quantitatively evaluated on the scintigraphic images, in comparison with identical dimension background aria. The maximum uptake observed was considered 100% (founded to correspond to the stomach region at 4 h for ^{99m}Tc-SNPs) and all the other measured uptakes were calculated as percentages in reference to the maximum, per g organ. Data were graphically represented, making evidence of ^{99m}Tc-SNPs biodistribution. Same data were obtained on the free ^{99m}Tc biodistribution images, for the control group.

Fig. 6 reveals, graphically, the significant difference in biodistribution between ^{99m}Tc labelled nanoparticles prepared by sodium borohydride method and free ^{99m}Tc. The ^{99m}Tc-SNPs exhibited higher uptake in all the investigated organs (27–100% count/g organ at 4 h) as compared to free ^{99m}Tc images (in the range of 18–88% count/g organ at 4 h).

In the case of free ^{99m}Tc (Fig. 6A), a discreet (17–20% count/g organ) area of fixation corresponding to thyroid was observed at all times (from 30 to 240 min). Also, a high uptake (with diffuse character on the scintigraphic images) was quantified in the upper abdominal region (63–88% count/g organ). Fixation consistent to the bladder region was also present (16–88% count/g organ), behavior that can be explained by the fact that the radiotracer was extensively excreted by urine.

The obtained quantified results (Fig. 6B) showed that in the case of ^{99m}Tc labelled nanoparticles, after 30 min, reached systemic circulation and were captured mainly in the salivary glands (51%

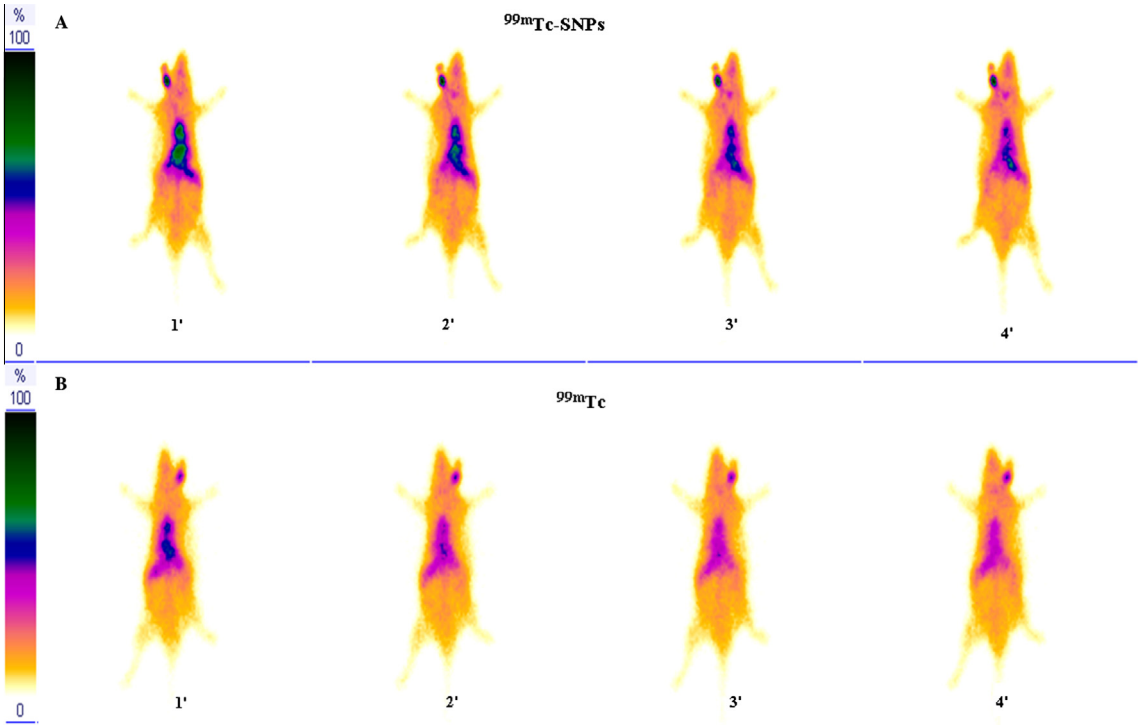

Fig. 7. Scintigraphic images after immediately *i.v.* administration of A. ^{99m}Tc-SNPs and B. free ($^{99m}TcO_4^-$).

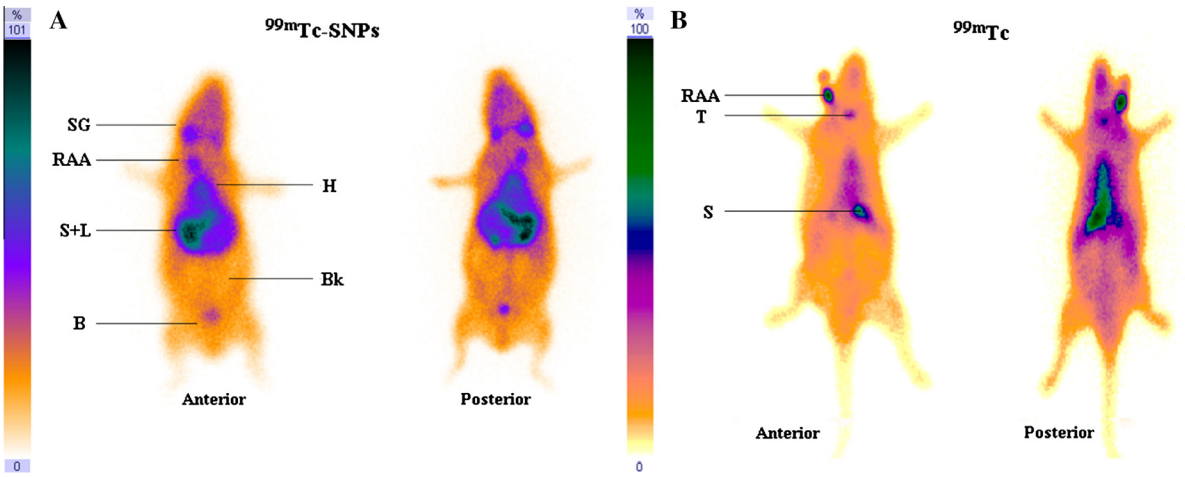

Fig. 8. Scintigraphic images at 30 min post injection of A. ^{99m}Tc-SNPs and B. free ($^{99m}TcO_4^-$). The values explain the image heterogeneity: SG - salivary glands; T - thyroid gland; H - heart; S + L - stomach and liver; B - bladder; RAA - radiotracer administration aria; Bk - background.

count/g organ), stomach (75% count/g organ), and kidney (37% count/g organ) in addition to a significant accumulation in the bladder region (28% count/g organ). This behavior was also observed at times of 60 and 240 min after injection, as it was expected, due to the nature of the injected compound.

One hour after injection, the ^{99m}Tc-SNPs were accumulated in all investigated organs and animal tissues, except in the thyroid. We also found that, within 4 h after injection, silica nanostructures undergo an increasing accumulation in the stomach (100% count/g organ).

The scintigraphic examination has also evidenced an important percentage (13 and 9% count/g organ for right and left eyeball, respectively, at 30 min) of ^{99m}Tc-SNPs in the eyeballs with an increasing trend in time (27 and 36% count/g organ for right and left eyeball, respectively, at 4 h).

After 4 h, a low percentage of the injected dose could be observed in the liver. This conduct could be explained probably by the fact that SNPs can be metabolized in the body due to the pH-dependent dissolution process that can occurs in aqueous solutions. The fixation corresponding to the urinary bladder also decreases gradually due to the radiotracer's elimination in the urine and also biological and physical half-life of the radioisotope.

These graphically results are validated by studying the gamma scintigraphic images of guinea pigs as shown in Fig. 7. The dynamic scintigraphic images (Fig. 7) showing localization of ^{99m}Tc-SNPs and free ^{99m}Tc in different organs, taken in the first 5 min (Fig. 7A and B), sustained the *in vivo* biodistribution profile observed on the static images and quantified on the graphs.

After 30 min post-tail injection (Fig. 8), the scintigraphic images showed the rapidly accumulation of ^{99m}Tc-SNPs in the salivary

glands, stomach, kidney and bladder region, which is in accordance with the fluorescent biodistribution study. These results are consistent with data published in the last years (Pandey et al., 2014; Simone et al., 2012; Xie et al., 2010) in a previous studies performed on radiolabelled nanoparticles.

The most important difference is the presence of the free ^{99m}Tc fixation area corresponding to thyroid observed at all times (from 30 to 240 min), but not evidenced on the ^{99m}Tc-SNPs images. These images can be explained by the known cellular uptake mechanism of the free ^{99m}Tc: the radioisotope is taken up via sodium iodide symporter system (NIS), a transmembrane transport system that was find to mediate the transport and cellular accumulation of both iodine and ^{99m}Tc to some tissues including mainly the thyroid, but also stomach, salivary glands, and to some extent the small intestine (Kiratli et al., 2009; Mu et al., 2012). Our SNP carrying amino groups on their surface are also electrically charged. Due to their small size and ionic charge, it is very likely that a passive transport is involved, according to the electrochemical gradient. In fact, the lack of the thyroid scintigraphic uptake for the SNP sustains the hypothesis of different transmembrane transport mechanisms for the radiotracer. The ^{99m}Tc-SNPs rapidly appear in the tissues, faster when compared to the ^{99m}Tc. This could be explained in relation their smaller size which gives them the possibility to a faster transmembrane passage. However, more detailed studies regarding the bioaccumulation of SNPs in the liver, spleen, intestines, kidneys, and bladder is warranted to better clarify the adverse effects arising from such an accumulation.

Considering the results obtained in our study, the SNPs showed *in vivo* similar biodistribution behavior to that demonstrated by others groups on nanostructured systems as silica nanoparticles (obtained by the same method) or chitosan nanoparticle, when the radioactivity was determined by scintigraphy (Banerjee et al., 2005; Xie et al., 2010). (Sakai et al. (2012)) analyzed the whole-body distribution of ^{14}C-ADP-labeled silica nanoparticles after intravenous injection into mice and the obtained radioactivity results showed also similar distribution patterns when determined by liquid scintillation counter.

Identifying the specific biodistribution areas (compared with free ^{99m}Tc) could be the start point for the use of this nanostructure system as vector molecule for a certain radioisotope, to be used for diagnosis in nuclear medicine imaging (using a classical gamma emitter radioisotope, such as ^{99m}Tc) and, respectively, therapy (using a suitable corpuscular emitter radioisotope such as ^{131}I) purposes.

4. Conclusions

In the present investigation, spherical bare, amino functionalized, Cy.5.5 fluorescent and ^{99m}Tc radiolabelled SNPs were successfully synthesised by the hydrolysis reaction of TEOS in ethanol containing water and ammonia. Particle sizes in the range of 200–350 nm, as determined by field emission SEM analysis, as well as the physico-chemical properties made the obtained SNPs potential candidates for *in vivo* studies. No significant signs of toxicity of the administered SNPs at a dose of 100 mg/kg bw were noted, proving a good level of safety for the tested nanoparticles. Using confocal microscopy technique, we demonstrated the high uptake of fluorescent SNPs in all the investigated organs (liver, kidney, testis, spleen and lung) for both oral and intravenous administration. The results of radiolabelled biodistribution indicated that ^{99m}Tc-SNPs accumulated mainly in salivary glands, stomach, kidney and bladder region and retained in these tissues for over 240 min. Collectively, the obtained radiolabelled SNPs exhibited high labelling efficiency and stability along with their biodistribution. Future work should focus on the ultimate combination of diagnostic and therapeutic capabilities of the functional SNPs with reduced toxicity, low level of side effects and a reduced cost, starting with understanding ^{99m}Tc-SNPs tissular uptake mechanisms.

Acknowledgements

Work partially supported by the Romanian Ministry of Education and Science, grant CNCSIS IDEI 1734/2009. The authors would like also to thank to Radu Iliescu, Catalina Roxana Bohotin and Ionut Tudorancea for their time and advices for improving the manuscript.

References

Argyo, C., Weiss, V., Bräuchle, C., Bein, T., 2014. Multifunctional mesoporous silica nanoparticles as a universal platform for drug delivery. Chem. Mater. 26, 435–451.

Banerjee, T., Singh, A.K., Sharma, R.K., Maitra, A.N., 2005. Labeling efficiency and biodistribution of Technetium-99m labeled nanoparticles: interference by colloidal tin oxide particles. Int. J. Pharm. 289, 189–195.

Barnes, C.A., Elsaesser, A., Arkusz, J., Smok, A., Palus, J., Lesniak, A., Salvati, A., Hanrahan, J.P., Jong, W.H., Dziubaltowska, E., Stepnik, M., Rydzyński, K., McKerr, G., Lynch, I., Dawson, K.A., Howard, C.V., 2008. Reproducible comet assay of amorphous silica nanoparticles detects no genotoxicity. Nano Lett. 8, 3069–3074.

Digigow, R.G., Dechézelles, J.-F., Dietsch, H., Geissbühler, I., Vanhecke, D., Geers, C., Hirt, A.M., Rothen-Rutishauser, B., Petri-Fink, A., 2014. Preparation and characterization of functional silica hybrid magnetic nanoparticles. J. Magn. Magn. Mater. 362, 72–79.

Garg, M., Garg, B.R., Jain, S., Mishra, P., Sharma, R.K., Mishra, A.K., Dutta, T., Jain, N.K., 2008. Radiolabeling, pharmacoscintigraphic evaluation and antiretroviral efficacy of stavudine loaded 99mTc labeled galactosylated liposomes. Eur. J. Pharm. Sci. 33, 271–281.

Hong, H., Zhang, Y., Sun, J., Cai, W., 2009. Molecular imaging and therapy of cancer with radiolabeled nanoparticles. Nano Today 4, 399–413.

Kamarudin, N.H.N., Jalil, A.A., Triwahyono, S., Salleh, N.F.M., Karim, A.H., Mukti, R.R., Hameed, B.H., Ahmad, A., 2013. Role of 3-aminopropyltriethoxysilane in the preparation of mesoporous silica nanoparticles for ibuprofen delivery: effect on physicochemical properties. Micropor. Mesopor. Mater. 180, 235–241.

Kiratli, P.O., Aksoy, T., Bozkurt, M.F., Orhan, D., 2009. Detection of ectopic gastric mucosa using 99mTc pertechnetate: review of the literature. Ann. Nucl. Med. 23, 97–105.

Kong, B., Seog, J.H., Graham, L.M., Lee, S.B., 2011. Experimental considerations on the cytotoxicity of nanoparticles. Nanomedicine 6, 929–941.

Legrand, S., Catheline, A., Kind, L., Constable, E.C., Housecroft, C.E., Landmann, L., Banse, P., Pieles, U., Wirth-Heller, A., 2008. Controlling silica nanoparticle properties for biomedical applications through surface modification. New J. Chem. 32, 588–593.

Lewinski, N., Colvin, V., Drezek, R., 2008. Cytotoxicity of nanoparticles. Small 4, 26–49.

Loudos, G., Kagadis, G.C., Psimadas, D., 2011. Current status and future perspectives of in vivo small animal imaging using radiolabeled nanoparticles. Eur. J. Radiol. 78, 287–295.

Lu, J., Liong, M., Zink, J.I., Tamanoi, F., 2007. Mesoporous silica nanoparticles as a delivery system for hydrophobic anticancer drugs. Small 3, 1341–1346.

Mamaeva, V., Sahlgren, C., Lindén, M., 2013. Mesoporous silica nanoparticles in medicine – Recent advances. Adv. Drug Deliv. Rev. 65, 689–702.

Md, S., Khan, R.A., Mustafa, G., Chuttani, K., Baboota, S., Sahni, J.K., Ali, J., 2013. Bromocriptine loaded chitosan nanoparticles intended for direct nose to brain delivery: pharmacodynamic, pharmacokinetic and scintigraphy study in mice model. Eur. J. Pharm. Sci. 48, 393–405.

Morales-Avila, E., Ferro-Flores, G., Ocampo-García, B.E., Ramírez, F.-M., 2012. Radiolabeled nanoparticles for molecular imaging. In: Schaller, Bernhard (Ed.), Molecular Imaging. InTech, pp. 15–38.

Mu, Q., Hondow, N.S., Krzemiński, L., Brown, A.P., Jeuken, L.J.C., Routledge, M.N., 2012. Mechanism of cellular uptake of genotoxic silica nanoparticles. Part Fibre Toxicol., 9–29

Napierska, D., Thomassen, L.C., Rabolli, V., Lison, D., Gonzalez, L., Kirsch-Volders, M., Martens, J.A., Hoet, P.H., 2009. Size-dependent cytotoxicity of monodisperse silica nanoparticles in human endothelial cells. Small 5, 846–853.

Newman, S.P., Hirst, P.H., Wilding, I.R., 2003. New developments in radionuclide imaging for assessing drug delivery in man. Eur. J. Pharm. Sci. 18, 19–22.

Pandey, U., Kameswaran, M., Dev Sarma, H., Samuel, G., 2014. ^{99m}Tc carbonyl DTPA–Rituximab: preparation and preliminary bioevaluation. Appl. Radiat. Isotopes. 86, 52–56.

Peer, D., Karp, J.M., Hong, S., Farokhzad, O.C., Margalit, R., Langer, R., 2007. Nanocarriers as an emerging platform for cancer therapy. Nat. Nanotechnol. 2, 751–760.

Sakai, N., Takakura, M., Imamura, H., Sugimoto, M., Matsui, Y., Miyoshi, H., Nakayama, A., Yoneda, M., 2012. Whole-body distribution of ^{14}C-labeled silica nanoparticles and submicron particles after intravenous injection into mice. J. Nanopart. Res. 14, 849–859.

Sarparanta, M., Mäkilä, E., Heikkilä, T., Salonen, J., Kukk, E., Lehto, V.-P., Santos, H.A., Hirvonen, J., Airaksinen, A.J., 2011. ^{18}F-labeled modified porous silicon particles for investigation of drug delivery carrier distribution in vivo with positron emission tomography. Mol. Pharm. 8 (5), 1799–1806.

Simone, E.A., Zern, B.J., Chacko, A.M., Mikitsh, J.L., Blankemeyer, E.R., Muro, S., Stan, R.V., Muzykantov, V.R., 2012. Endothelial targeting of polymeric nanoparticles stably labeled with the PET imaging radioisotope iodine-124. Biomaterials 33, 5406–5413.

Slowing, I.I., Trewyn, B.G., Giri, S., Lin, V.S.Y., 2007. Mesoporous silica nanoparticles for drug delivery and biosensing applications. Adv. Funct. Mater. 17, 1225–1236.

Stober, W., Fink, A., Bohn, E., 1968. Controlled growth of monodisperse silica spheres in the micron size range. J. Colloid Interface Sci. 26, 62–69.

Wu, X., Wu, M., Xiaojun Zhao, J., 2014. Recent development of silica nanoparticles as delivery vectors for cancer imaging and therapy, a review. Nanomed. Nanotech. Biol. Med. 10, 297–312.

Xie, G., Sun, J., Zhong, G., Shi, L., Zhang, D., 2010. Biodistribution and toxicity of intravenously administered silica nanoparticles in mice. Arch. Toxicol. 84, 183–190.